Chemical Physics Impact 5 (2022) 100130

Contents lists available at ScienceDirect

Chemical Physics Impact

journal homepage: www.sciencedirect.com/journal/chemical-physics-impact

Investigating the physicochemical properties and pharmacokinetics of curcumin employing density functional theory and gastric protection

Suhailah Wasman Qader [a,*], A. Suvitha [b], Mehmet Ozdemir [c], Innocent Benjamin [e,g,*], Anu Sai Ram NSA [d], Martilda U. Akem [e,f], Ahuekwe Eze Frank [e,h], Emereze C. Eluwa [e]

[a] Department of Medical Laboratory Science, Knowledge University, Erbil, Iraq
[b] Department of Physics, CMR Institute of Technology, Bengaluru-560037, Karnataka, India
[c] Department of Dentistry, Tishk International University, Erbil, Iraq
[d] Department of Medicine, Tirunelveli Medical College, Tamil Nadu, India
[e] Computational and Bio-Simulation Research Group, University of Calabar, Calabar, Nigeria
[f] Department of Pure and Applied Chemistry, Faculty of Physical Sciences, University of Calabar, Calabar, Nigeria
[g] Department of Microbiology, Faculty of Biological Sciences, University of Calabar, Calabar, Nigeria
[h] Department of Biological Sciences, Covenant University

ARTICLE INFO

Keywords:
Curcumin
Pharmacokinetics
DFT
Gastric protection
Physicochemical characteristics

ABSTRACT

The extraction, isolation as well as theoretical investigation of Cumcuma Xanthoriz (cxz) molecule was evaluated to ascertain the physicochemical properties (pc) of the investigated compound. The plant extracts were isolated and characterized using NMR, FT-IR and UV-Vis Spectroscopy study. Pre-geometry characterization as well as theoretical analysis were performed within the frame of density functional theory (DFT) at B3LYP/6-311++ G (d,p) level of theory. Global descriptors were calculated at the same level of theory to ascertain the molecular stability, chemical reactivity of the investigated molecules. Stabilization studies was conducted to properly evaluate the stability of the complex and as such, the result obtained divulged that the charge delocalization from sigma (σ) to anti-sigma (σ*) molecular orbital contributed chiefly to the molecular stability of the studied compound. The calculated UV-Vis spectroscopy study reveal that all absorption spectrum occurred at the visible region (400nm-700nm) which correlate with the experimental λmax obtained. Excitation of CXZ was observed to emanate from π→π*electronic transition. Result from the topology and admet properties explicates that CXZ molecule exhibited good ADMET properties and therefore suggests its suitability as potential plant based drug.

1. Introduction

A wide range of biological and pharmacological effects of curcumin have been documented, including anti-inflammatory, antioxidant, antibacterial, anti-diabetic, anti-cancer, anti-rheumatic, anti-thrombotic, and hepato-, nephro-, and cardiac protective effects. Curcumin has been shown to be exceedingly safe, even at very large dosages, in a number of animal models and human investigations [1,2]. The molecule has equally demonstrated to possess potential ingredients for the treatment and prevention of a wide range of human disorders due to its pharmacological safety and efficacy as reported by [3]. Interestingly, curcumin is thought to be a potential component of functional diets. Over the years, findings have demonstrated curcumin's hyperglycemic action, pointing to the possibility of using curcumin in foods for people with diabetes [4]. It has also been proven to be a natural compound with multiple uses that is pharmacologically safe and has been shown to have cytoprotective effects on healthy human cells [5]. However, in order to get beyond the solubility and bioavailability issues related to curcumin, computational analysis may be utilized as a guide for pre-formulation prospective. The potential targets of curcumin-modified conjugates (CMCs) in breast cancer cells were identified by molecular docking investigations, which initially stipulated that the clinical constraint of employing curcumin as possible anticancer medications, is established that curcumin conjugates have a considerable anticancer property at a sub-micromolar concentration according to a study by Panda and colleagues [6]. On the other hand, Ahmed et al [7] also examined into the biological effects of curcumin, which revealed that the molecular docking predicted binding modes indicated that curcumin binds with

* Corresponding authors.
E-mail addresses: suhailawasman@gmail.com (S.W. Qader), benjamininnocent53@gmail.com (I. Benjamin).

https://doi.org/10.1016/j.chphi.2022.100130
Received 30 August 2022; Received in revised form 9 November 2022; Accepted 20 November 2022
Available online 25 November 2022

the hCA-1 enzyme, thus suggesting efficient pharmalogical effects on target receptors. Additionally, according to Furlan and colleagues [8], the structural characteristics of these potential compounds were explored using DFT studies, in their studies keto and enol isomers of indole curcumin derivatives were compared and energy analysis suggested that enol isomers were more stable than the keto isomers. Also, it was discovered that the result gotten from the molecular docking shows that the keto form of indole curcumin molecules were efficiently binding with GSK.3B, EGFR, and BCR-ABL proteins which implies that they possess significant anti cancer activity. Kumar, and colleagues [9] further explained that in other to examine and study the potentials of curcunin in cancer prevention and treatment, they carried out systematic absorption studies of curcumin and anti cancer drugs on montmorillnite(MMT) nanoparticles in the presence of amphiptilic polymer (PLGA)and in an aqueous environment to understand the contribution of the layered clay structure using cluster(B97-D), DFT and molecular dynamics (MD) simulation in acidic and natural p^H-media. It was found out that(MMT) has affinity towards either polymers or drug molecules.

However, in order to better understand the structure and reactivity of this potent drug, it is imperative to analyze the nature of many of the biological aspects of this prescription, many of which are yet unknown [10–14]. Although, curcumin has not yet received approval as a medicinal agent despite its efficacy and safety, and its poor bioavailability has been cited as a key issue for this as documented by [15,16]. The main causes of curcumin's poor bioavailability include low absorption, quick metabolism, and swift excretion. The research of illness progression, comprehension of drug-organism interactions, and directing of novel drug discovery are all addressed by network pharmacology, a systems biology approach [17]. Significantly, in recent years, a number of studies have reported the use of advanced computational methods, including density functional theory (DFT), to effectively elucidate the structural and chemical properties of compounds in order to develop therapeutics for a variety of diseases. Additionally, molecular docking is used to accurately take into account the compatibility between the drugs and the target receptors. ADME investigations utilizing software such as SWISSADME, pkcSM, etc. are used to assess the rate at which these compounds are absorbed, distributed, metabolized, and excreted.

Herein, the study employs a high-level computational analysis of Curcumin utilizing density functional theory (DFT) approach optimized at B3LYP/6-311++G(d,p) level of theory. Accurate quantum mechanical studies on Curcumin, are here carried out with the aim to analyze the conformational equilibria, to find the most stable equilibrium structure and to define the nature of the molecular orbitals, particularly the highest occupied and lowest unoccupied (frontier molecular orbital) ones that are important to explain binding characteristic. NMR, UV–vis and FTIR both theoretical and experimental data are employed in the comparison with electronic and conformational properties of Curcumin. These probes must also meet certain topological and ADMET property requirements in order to be of interest and well as the molecular docking analysis. This study predicts the standard physicochemical properties (PC) to account for a variety of Absorption, Distribution, Metabolism, Excretion, and Toxicity (ADMET) parameters including molecular lipophilicity, topology, and the Bioactivity Radar to aid drug development using online servers and well-established commercial software.

2. Experimental

2.1. Synthesis

The dried leaves of Curcuma xanthorrhiza (Roxb) were purchased from Ethno Resources Sdn Bhd (846944-K). The plants were extracted using sterilized-distilled water (SDW)and ethanol (E) in a ratio of 1:20. Adult healthy male Sprague Dawley rats (150-200 g) were obtained from animal house, faculty of medicine, University of Malaya, Kuala Lumpur (Ethics No. PM 07/10/2009 MAA (a) (R)). During the laboratory experiment, rats were provided meticulously and care aligned with respect to the standards addressed in the "Guide for the Care and Use of Laboratory Animals" published by the National Academy of Sciences and published by the National Institute of Health. Briefly, the rats were further separated into two groups after being deprived of food for 24 hrs. The animals were then orally administered with the plant extracts for antiulcer assessment separately the details explained in Tables 1 and 2.

2.2. Spectroscopy

On a Bruker Avance AMX400 spectrometer using a Broad Band 5-mm probe, NMR spectra are captured at 300 K. (inverse detection). The conventional frequencies for 13C and 1H are respectively 100.13 MHz and 400.13 MHz. The following are the typical acquisition parameters for 1 H: Spectral bandwidth (SW) of 20 ppm, pulse width of 6.1 ls (90-pulse hard pulse on 1 H), pulse latency of 0.5–1 s, and scan count of 216–512. Typical settings were employed for 2D H, H-Homonuclear Correlated Spectroscopy (COSY). Appropriate settings were employed for 2D H, X-Hetero Correlated Spectroscopy (HMBC and HMQC). (50–90 pulses; 32 k data points; 1 s relaxation delay; 8–64 k transients; 1 JH–C 125–145 Hz; 3 JH–C 5–15 Hz). The B3LYP approach was used to determine the electronic transition for the CXZ, with the base 6-311++G (d, p) set to UV-visible spectral computation and the gaseous phase included. Between 300 and 800 nm, the theoretical UV-visible absorption spectrum was measured in the gaseous phase.

2.2.1. Computational details

Time-dependent DFT (TD-DFT) calculations were performed on the compound *Curcuma xanthorrhiza* to optimize the structure in the ground state (shown in Fig. 1) at Becke's three-parameter functional and Lee-Yang-Parr hybrid functional (B3LYP) level at 6-311++ G(d, p) basis set using both Gaussian (G09) [18] and GaussView 6 [19] programs. To perform UV-Vis spectral computations that are applied to optimal structures, TD-DFT/B3LYP/6-311++G (d, p) was utilized. Comparative physical indices such as E_{HOMO}, E_{LUMO}, offset HOMO/LUMO, MEP, spin, ionizing-potential (I), electronic-affinity (A), chemical-potential (μ), hardness (η), electrophilic-index (ω), softness (ζ) measurements of the gaseous phase are measured.

2.2.2. Molecular docking details

Herein, the downloaded protein (PDB ID: 1BZM) was prepared using the Biovia Discovery Studio and docked with the compound under investigation (curcumin) and further validated by docking same with the conventional drug (omeprazole). To sequentially prepare the protein before carrying the molecular docking proper, water molecules present in the proteins were deleted and the active binding sites were defined from the current ligand site after which the native ligand present in the protein was deleted. The binding site was expanded to cover more area and the polar hydrogens were added to the structure and saved in PDB format. The sphere's radius and coordinates were copied in order to dock. The PDB formatted proteins that had been saved were chosen from the read molecule tab of the Autodock Vina software. The grid and macromolecule icon were chosen, the protein was chosen as a

Table 1
Effect of aqueous extract of selected Malaysian medicinal plants on ulcer area and percentage inhibition of ethanol induced gastric ulcer rats.

Pre-treated dose (5 mL/kg)	^H_P	Ulcer area(mm)^2 (Mean ± S.E.M)	Inhibition (%)
DW (negative ulcer control)	3.45 ± 0.13	865.3 ± 42.4	-
OMP (positive control 20 mg/kg)	6.84 ± 0.17*	114.4 ± 3.71*	86.77
▓CXLAE (250 mg/kg)	4.03 ± 0.14*	314.9 ± 7.40*	63.60
▓CXLAE (500 mg/kg)	4.50 ± 0.12*	224.9 ± 9.24*	74.00

Table 2
Effect of ethanol extract of selected Malaysian medicinal plants extract on ulcer area and percentage inhibition of ethanol induced gastric ulcer rats.

Pre-treated dose (5 mL/kg)	$^{H}_{P}$	Ulcer area(mm)^2 (Mean ± S.E.M)	Inhibition (%)
CMC (negative ulcer control)	3.60 ± 0.10	978.3 ± 32.4	-
OMP (positive control 20 mg/kg)	6.84 ± 0.17*	114.4 ± 3.71*	88.30
CXLEE (250 mg/kg)	4.25 ± 0.10*	91.10 ± 9.29*	90.68
CXLEE (500 mg/kg)	5.10 ± 0.23*	81.70 ± 7.29*	91.64

macromolecule, and the file was saved in pdbqt format. The required ligand in pdb format was selected once the ligand icon was clicked. The ligand was loaded, and the ligand and output tab was chosen to save the ligand in pdbqt format. Results were acquired using the Biovia discovery studio visualizer.

3. Results and discussions

3.1. Geometry optimization

The highly symmetrical and conjugative nature of Curucuma xanthorhiz (CXZ) accounts for its versatility and utilization in diverse applications. Several derivatives have been isolated and reported. The structure is composed of 8 rotatable bonds interwoven between two aromatic rings with 6 acceptors and 2 donor groups which are responsible for the ease of inter-conversion from the keto to the enol tautomer and vice versa. It is synonymous to the compound 1 1, 6-Heptadiene-3, 5-dione, 1,7-bis(4-hydroxy-3-methoxyphenyl). However, to accurately predict molecular properties and assess the bio-activity of the studied compound, geometry optimization was ensured at the B3LYP functional with the 6-311++G (d, p). The molecule is observed to possess 4 distinct bonds. The C=O bond length is computed to be – while the aromatic C=C bond is observed to be—similarly as well as the OH. The bond lengths suggest therefore that the title compound poses a great inhibitory potential on target receptors.

3.2. NMR spectra

The experimental ^{1}H NMR spectra of the titled compound in DMSO-d_6 as a solvent confirmed the presence of suspect protons. A comparison of the experimental and calculated spectra is represented in **Fig S1** and **S2** of the supporting information. The aromatic protons found in the test compound, for the experimental, appeared at 6.86-7.63 ppm, while the number of protons calculated showed 7.20-8.89 ppm. This depicts the presence of protons among aromatic and heteroaromatic rings duplicated in their expected regions [20,21]. The variations in protons signal may be attributed to varied behaviour to the ions in the compound [22]. The ^{1}H NMR integration curves confirms the formation of keto-enol tautomers of the proposed structures in solution.

3.3. UV–visible& DOS spectral analysis

The results of the Gauss Sum software analysis of key contributions to electronic transfers are summarized in Table 3. Excitation energies E (eV) and oscillator strengths (f) were measured, as well as experimental absorption wavelength (nm) and major contribution (HOMO-LUMO). Fig. **S3** of the supporting information depicts a pictorial representation of theoretical UV-Vis Spectra and a DOS chart. While the investigated CXZ exhibited six absorption bands in the theoretical UV spectrum at 417,371,370,358,349 and 322 nm, this corresponded duly with the experimental λ (nm) as shown in Table 3. These results suggest that the investigated compound may be attributed to the aromatic, amino benzoate anion, monohydrate and oxalate moiety, respectively, these transformations could be contributed to the π→π*, n→π*, σ→σ* transition.

Table 3
Absorption wavelength λ (nm), excitation energies E (ev) and oscillator strengths (f) theoretical and experimental electronic absorption spectra using the process TD-DFT / B3LYP/6-311++ (d, p).

Molecule	λ (nm) Experimental	Theoretical λ(nm) Computed	E (eV)	*f* (a.u)	Major contribution
CXZ	416.8	417.3	2.96	0.0205	HOMO->LUMO (91%)
	421.3	471.2	3.33	0.3351	H-1->LUMO (85%)
	419.5	422.1	3.34	0.0175	H-5->LUMO (26%), H-3->LUMO (23%), H-2->LUMO (31%)
	358.0	375.1	3.45	0.0006	H-3->L+1 (68%), H-2->L+1 (21%)
	358.4	349.4	3.54	0.2495	HOMO->L+1 (88%)
	343.8	322.1	3.84	0.0003	H-1->L+1 (97%)

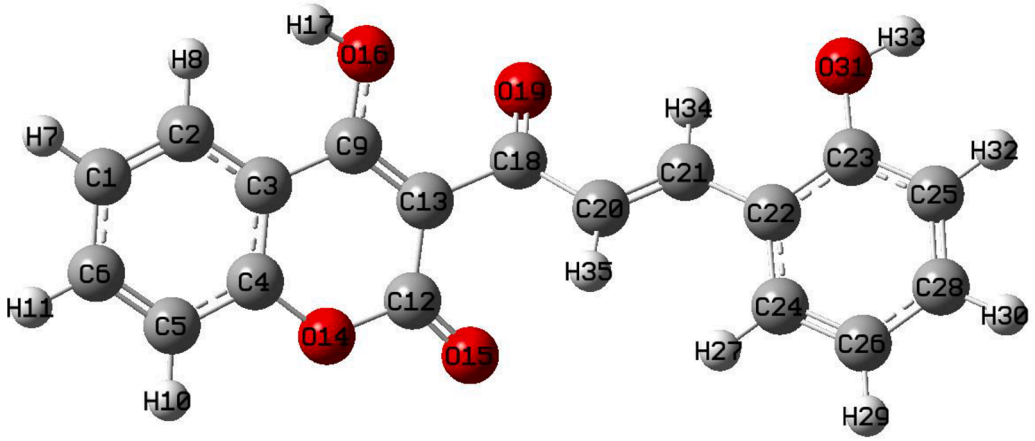

Fig. 1. Optimized Molecular Structure of CXZ.

3.4. Vibrational Analysis

Vibrational analyses aid in qualitative and quantitative characterization of test compounds. The FT-IR analysis assessed the functional group types present in the test compound, via distinct molecular vibrational bands for the respective functional groups present. The computationally calculated vibrational wavenumbers and experimental (FT-IR) measurements of the titled compound are presented in Table 4 and the spectra is illustrated in fig. S4 of the supporting information. To improve agreement between the theoretical and experimental values, and to compensate for the errors possibly arising from the basis set, the computed harmonic frequencies in line with their potential energy distribution are generally scaled for comparison [23]. However, observed slight variations could be attributable to solvation and different functional effects [24].

C – H vibrations:

Vibrational bands in aromatic compounds reveal C-H stretch peaks normally in the region of 2850-3100 cm^{-1} [25]. More so, the nature and position of substituents affect these vibrations. In this study, the experimental C-H stretch deformations were observed at 808.03, 960.38, 1025.87 and 1112.73 cm^{-1}, with the corresponding theoretical C-H stretch values giving 969.07, 1017.08, 1030.4 and 1119.81 cm^{-1}, respectively. This data shows the closeness of the calculated theoretical values to the experimental results. Significant wavelength deviations from the norm could arise from solvent effects, as well as antisymmetric stretching vibrations of aldehyde bonds due to varying bond lengths. Thus, leading to weak absorption peaks [26]. Another possible explanation would be that the vibrational shift of the CH bond interacting with metals (or other elements) was averaged out by the unchanged vibrational mode of the non-interacting CH bonds; indicated by weakened bonds which inadvertently result in a reduced wavelength [27].

C – C vibrations

C – C vibrations arise in the range between 1300-1000 cm^{-1} [28]. In this study, the experimental σC=C stretching vibration frequency deformations occurred at 1135.89 and 1151.30 cm^{-1} and theoretically at 1178.58 and 1183.46 cm^{-1}, respectively. For τ C = C, experimental and theoretical values fell at 1182.18 and 1201 cm^{-1}, respectively; while ωC = C reported 1203.39, 1232.72, 1274.73, and 1263.98, 1281.71, 1301.60 cm^{-1} for experimental and theoretical values respectively. Theoretical values were in good agreement with the experimental results.

C-O vibrations

The stretching frequency varied in both the symmetric and asymmetric bond types. Experimental and Theoretical vibration frequencies with $_{Sym}$C = O were observed at 1427.08, 1600.67, 1625.74, and 1435.06, 1801.30, 1837.93 cm^{-1}, respectively; while the υ_{AS}C = O gave 1506.17, 1587.16, and 1549.97, 1637.77 cm^{-1}, for both the experimental and theoretical values, respectively. Previous studies have reported variable C-C band stretches [29]. However, close theoretical values and experimental data were reported in this study.

O-H vibrations

The presence of inter or intra molecular hydrogen bonding in the molecules of O-H group makes for a large variation in wavenumber, intensity and bandwidth of the spectral vibrations. As such the O-H stretching vibration is expected in the wide range of 3380 ± 200 cm^{-1} [24,25]. For the theoretical values of the title compound appearing at 3903.04 and 3906.59, the υO – H stretching for the experimental data were in good agreement as pure stretching mode at 2846.48 and 3507.92 cm^{-1}.

Table 4
Analysis of the theoretical and experimental vibrational frequencies of curcumin.

Experimental	Absorbance	Theoretical	Transmittance	Assignment with PED%
808.03	0.482	969.07	1.45	υ_{AS}C-H (-75)
960.38	0.485	1017.08	0.26	υ_{AS}C-H (-79)
1025.87	0.442	1030.40	42.47	υ_{AS}C-H (-81)
1112.73	0.497	1119.81	45.74	υ_{AS}C-H (-79)
1135.89	0.451	1178.58	16.62	δC=C (38)
1151.30	0.614	1183.46	7.35	δ C = C (31)
1182.18	0.457	1201.50	31.02	τ C = C (48)
1203.39	0.488	1263.98	202.03	ωC = C (37)
1232.72	0.383	1281.71	22.55	ωC = C (28)
1274.73	0.384	1301.60	76.33	ωC = C (49)
1427.08	0.477	1435.06	210.61	υO=C (24)
1506.17	0.491	1549.97	74.69	υO=C (30)
1587.16	0.212	1637.77	180.85	υO=C (29)
1600.67	0.249	1801.30	215.72	υO=C (34)
1625.74	0.242	1837.93	713.65	υO=C (36)
2846.48	0.049	3903.04	105.58	υO – H (49)
3507.92	0.085	3906.59	110.96	υO – H (55)

3.3. Frontier Molecular orbital (FMO) analysis

The HOMO and LUMO energy values can be used to determine a molecule's ability to donate and receive electrons. Electrical and optical properties, luminescence, photochemical reactions, UV-VIS, quantum chemistry, and pharmaceutical research, as well as providing information on biological mechanisms, rely on these molecular orbitals [26–28]. Frontier molecular orbitals (FMOs) energies such as I=-Energy HOMO and A= -Energy LUMO, according to Koopmans' definition, measure ionization1 potential (I) and electron affinity (A). A compound's chemical reactivity is believed to be determined by the energy gap, which is established by the difference between the energies of HOMO-LUMO. It has been demonstrated that a molecule's energy gap impacts its chemical reactivity, biological activity, polarizability, and susceptibility to bind compounds to target receptors [29]. The investigated compound revealed a very significant energy gap of 3.437 eV which in comparison with other literatures suggest that this compound possesses sufficient biological properties [30]. This assertion was significantly supported by the slight decrease in energy gap (2.886 eV) established in the docked complex with a difference of 0.551 eV. Importantly, a study carried out by Das and colleagues [31] revealed that at the binding site, the HOMO orbitals of the ligand interact with the LUMO orbitals of the amino acid residues. When a complex is formed, however, HOMO orbitals of the binding site residues interact with LUMO orbitals of the ligand. Additionally, the active site loop of Lys213, Glu214, Lys149, and Ser217 were found to be essential for binding of the drug candidate due to its significant atomic displacements and intra-molecular hydrogen bonding. Herein, with the aid of the energies of the HOMO and LUMO orbitals, other examinations of the investigated molecule's chemical reactivity parameters, including chemical softness (S), chemical potential (μ), electrophilicity index (ω), and chemical hardness (η), were also performed as shown in Table 5. Additionally,

Table 5
Analysis of the electronic properties of CXZ.

Parameters	B3LYP_6–311++G(d,p)
Electronic spatial extent (au)	21174.8
nuclear repulsion energy (Hartree)	2110.17
Rotational coefficients (GHz)	0.2857
	0.053
	0.047
Dipole moment	2.611debye
Parameters	
$\mathbf{E_{LUMO}}$ (eV)	-2.6716
$\mathbf{E_{HOMO}}$ (eV)	-6.1086
Energy Gap (eV)	3.437
$\mathbf{I = -E_{HOMO}}$ (eV)	6.1086
$\mathbf{A = -E_{LUMO}}$ (eV)	2.6716
$\eta = \frac{1}{2}(E_{LUMO}-E_{HOMO})$ (eV)	1.7185
$\mu = \frac{1}{2}(E_{LUMO}+E_{HOMO})$ (eV)	-4.3901
$\psi = \mu^2/2\eta(eV)$	5.607
$\zeta = 1/\eta(eV^{-1})$	0.5819

according to [32], a molecule's electrophilicity index provides information regarding how well a substance can bind to biomolecules. The molecule in question has a higher electrophilicity index value, indicating that it can act as an electrophilic species and has a greater ability to bind to biomolecules and thus, confirms the pathway for molecular docking approach with different protein targets. Conversely, a soft molecule with strong polarizability has a lower chemical hardness value and a higher negative electrochemical potential (μ) indicates a chemical species' willingness to accept electrons while electronegativity (χ) measures the capacity of an atom/group of atoms to attract electrons in the molecule. Interestingly, results calculated validated the biological relevance of the compound under investigation as shown in Table 4. More so, the electron occupied and unoccupied (electron affinity and donating) sites are shown in 3D representations of FMO orbitals in different transitions (HOMO-LUMO) levels in Fig. 2.

3.4. Natural Bond Orbital (NBO) analysis

The NBO analysis relies on a series of methods that allow for the extraction of fundamental bonding concepts from density functional theory (DFT) calculations. It facilitates the conversion of the Schrodinger's wave equations' computational keys [33,34]. For the clarification of hyperconjugative interactions and the delocalization of electron density in the solvent, natural bond orbital analysis is a suitable tool. It is also a reliable technique for analyzing intra- and intermolecular bonding and interactions within bonds. The second- order perturbation theory analysis of the Fock matrix was carried out to evaluate the donor-acceptor interactions in the NBO basis. The concentration of the donor-acceptor interaction was denoted by the second order stabilization energy, E^2. The larger value of E^2 indicates the stronger interaction between electron donors (i) and the electron acceptor (j) which signifies a more donating propensity from an electron donor to electron acceptor and hence, a higher degree of conjugation of the whole system [35]. NBO can be mathematically expressed as outlined in literature [36]

NBO analysis of the studied molecule, is tabulated in Table 6 showing a strong intermolecular hyper conjugative interaction. From the computational details, it is observed that the studied compound had highest donor to acceptor interaction from (donor) σC_{20} - C_{21} → σ*C28 - H30 (acceptor), σC_{18} - C_{20} → σ*C26 - C28, σC_{20} - H35→ *σC26 - C28

Table 6
Analysis of the natural bond orbital at.

Donor orbital	Occupancy	Acceptor orbital	Occupancy	E^2 Kcal/mol	E(j)-E(i)	F(i,j)
σC_{20} - C_{21}	1.98490	σ*C28 - H30	0.01051	594.04	1.89	0.946
σC_{18} - C_{20}	1.98338	σ*C26 - C28	0.02072	577.05	1.85	0.923
σC_{20} - H35	1.93623	*σC26 - C28	0.02072	427.47	1.58	0.741
σC_{20} - C21	1.98490	*σC26 - C28	0.02072	434.82	1.84	0.799
σC_{20} - H35	1.93623	*σC28 - H30	0.01051	405.90	1.63	0.736
σC18 - C20	1.98338	*σC28 - H30	0.01051	403.37	1.90	0.783
LP(1)O 15	1.97733	*σC26 - C28	0.02072	183.90	1.94	0.533
π*C2 - C3	0.27819	*πC1 - C6	0.20847	107.82	0.02	0.076
πC_{20} - C21	1.85399	*σC28 - H30	0.01051	98.11	1.43	0.346
LP(2)O 15	1.86743	*σC26 - C28	0.02072	91.37	1.44	0.333

which is found to have the highest the stabilization interaction of 594.04 Kcal/mol, while the occupancies explain the location of the donor electron or orbital in an atom. Hence, the interaction is between sigma bond to the sigma anti-bonding contributing greatly to the stability of the compound (cmr). Relatively, the highest perturbation energy results from the influence of the antibonding interaction between atoms, amounting in the increased molecular stability as seen in other stability descriptors. These stabilization interactions between the lone pair orbitals and the antibonding orbitals increases the stability of these compounds.

3.5. Mulliken and Natural Population Analysis (npa)

The natural population analysis accurately determined the distribution of electrons in various subshells of their atomic orbitals and their occupancies [37]. The system of natural population analysis has been established to estimate the atomic charges and orbital populations of

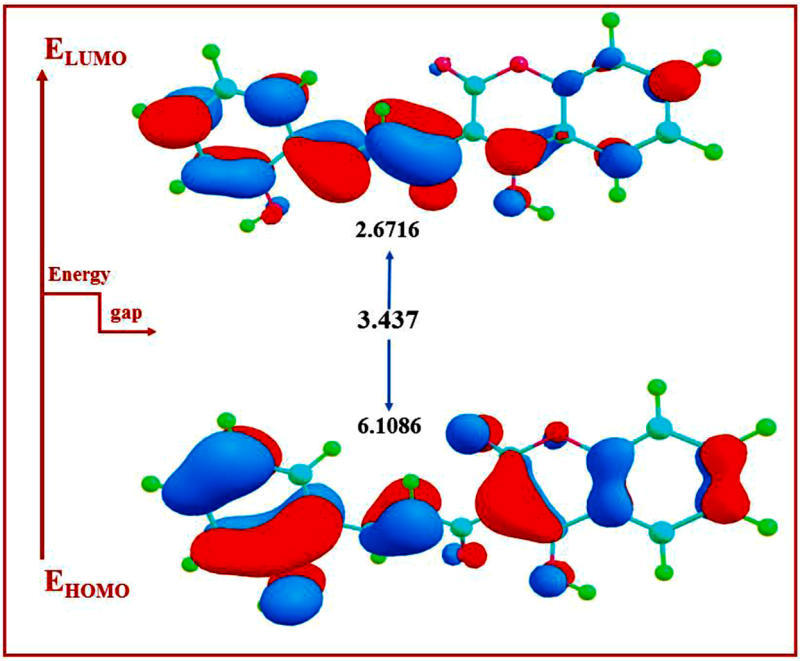

Fig. 2. DFT/B3LYP/6–311++G(d,p)-3D representations of FMO orbitals in (HOMO-LUMO) levels for CXZ.

molecular wave functions. Natural analysis is also an alternative to predictable Mulliken population analysis which appears to unveil and enhanced the numerical stability and to better describe the electron distribution in compounds of high ionic character, such as those comprising metal atoms [38]. These charges are seen to affect the properties like dipole moment, electronic parameters, polarizability, and refractivity [39]. The iso-surface of molecular electrostatic potential, determines the interacting strength of the compound, it is considered suitable for the prediction of the reactivity of the molecule towards nucleophilic and electrophilic occurrences [40–43]. It also predicts which category of intermolecular interactions is possible within the interacting system. From our studies, red color best explains the presence of dispersion force and negative charges with higher electron density, blue represent a positive charge with less electrostatic potential (electrophilic) while yellow signifies negative charge where high electrostatic potential resides.

On the other hand, the Mulliken population analysis, describes the distribution of the charges in the various sub shells in the molecular orbital. The atomic charge influences the polarizability, dipole moment, electronic structure and many other molecular properties of the system [36]. As reported in table S1 of the supporting information and Fig. 3. The Mulliken atomic charge can also be employed for the characterization of the electronic charge distribution in a particular molecule and also for the characterization of the bonding, antibonding and non-bonding nature of the molecular orbitals [37]. Herein, the Mulliken atomic charges cover a broad range of values from -0.429144 at the low side to 1.002035 at the high side at the Hartree-Fock level. The atoms C_3, H_7, H_8, C_9, H_{10}, H_{11}, C_{12}, C_{13}, H_{17}, C_{18}, C_{21}, C_{22}, C_{23}, H_{27}, H_{29}, H_{30}, H_{32}, H_{33}, H_{34}, and H_{35} respectively have positive charges and the atoms C_1, C_2, C_4, C_5, C_6, O_{14}, O_{15}, O_{16}, O_{19}, C_{20}, O_{24}, O_{25}, O_{26}, O_{28}, O_{31}, have negative charges. The hydroxyl oxygen O_{15} is more negative with value -0.429144 eV which is proved very strongly in Fig. 3.

3.6. Molecular electrostatic potential analysis

The MESP surface is extremely useful for understanding the potential sites for electrophilic (negative region) and nucleophilic (positive region) reactions [44,44], and it is particularly well suited for recognising one molecule by another via this potential and density, as shown in Fig. 4. Different shades represent the electrostatic potential levels at the surface in the order red > orange > yellow > gree n> blue. In the named compound, the colour code for these maps ranges from -1.533e^{-2} (deepest red) to +1.533e^{-2} (deepest blue), with blue representing the most electropositive, i.e. electron poor region, and red representing the most electronegative, i.e. electron rich region. The most electronegative region in the molecule is clearly around the three oxygen atoms, which act as an electron donor.

3.7. In silico ADMET analysis

According to the Lipinski's rule, which was used to clearly and unequivocally explain the drug-likeness and bioavailability capabilities of the investigated compound, it was examined that the compounds' absorption, distribution, metabolism, excretion, and toxicity properties made it clear that the molecules possess very reasonable pharmacokinetic features. This standard helps to assess the likelihood that a biologically active compound will have the chemical and physical properties required for absorption and bioavailability. The Lipinski rule is based on pharmacokinetic drug properties including molecular mass less than 500 Da, partition coefficient not greater than 5, and a maximum of 5 donors and 10 acceptors for hydrogen bonds. CXZ had a 368.38g/mol molecular weight. As a result, the Lipinski rule of five was strengthened by the findings that the minimum reported number of hydrogen bond donors was successful for oral administration. This outcome was in line with the information found on the number of hydrogen bond acceptors, which is provided in table X of the supporting data. In light of this, it is crucial to point out that after carefully examining the investigated compound, it is relevant to say that the molecule didn't violate any requirements, which implies that the molecule has excellent potential as an antimicrobial.

Additionally, no abnormalities in gastrointestinal (GI) absorption, blood brain barrier (BBB) permeability (a term used to describe the unique characteristics of the central nervous system (CNS) of microvasculature), P-gp substrate, CYPIA2, CYP2CI9, CYPP2D6, CYP3A4, Ghose, Veber, Egan, or Muegg were found by this examination, indicating that the molecule represents high hydrophilic properties and polar chemical as shown in Table 7. Therefore, the high potency, affinity, and selectivity against the molecular target were assessed in order to better understand the risky characteristics of the tested drugs. This led to the conclusion that CXZ was unlikely to be carcinogenic, mutagenic,

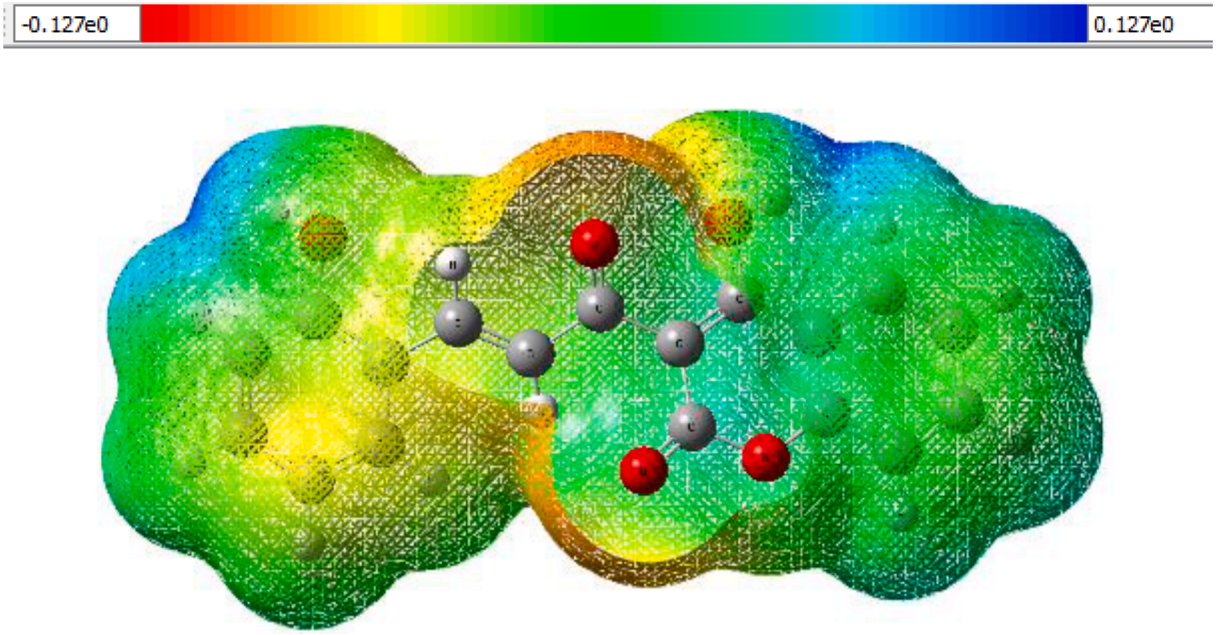

Fig. 3. Plot illustrating the mulliken and natural population analysis.

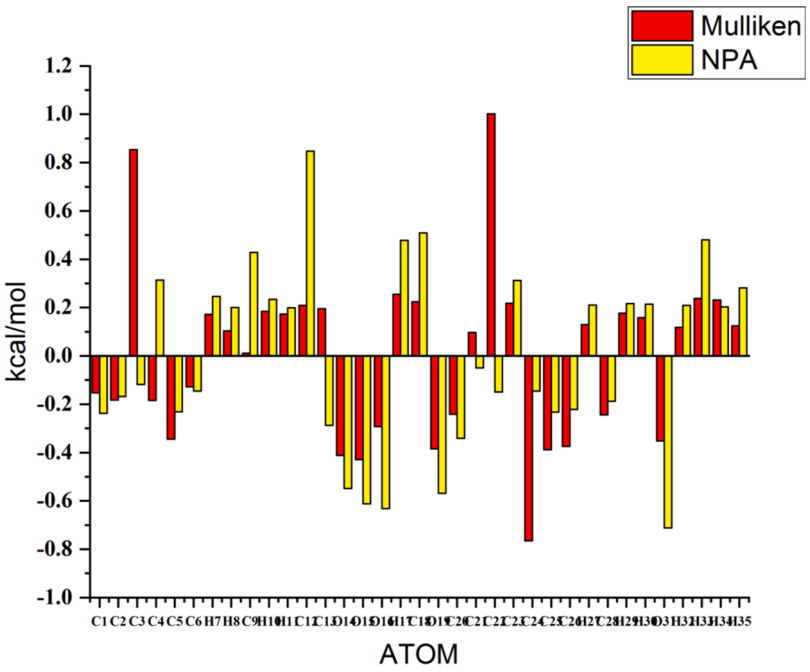

Fig. 4. Molecular electrostatic potential of studied CXZ compound.

or cytotoxic, with likelihood values of 0.62, 0.97, and 0.93, respectively as shown in table S8 of the supporting information. Significantly, this discovery implies that the lead compound possesses antimicrobial properties. The methoxy phenyl and heptadiene dione rings, which are highly significant in the antimicrobial activity, may be the source of this compound's remarkable biological power. The bioavailability radar, on the other hand, is shown to quickly assess how drug-like the molecule is.

3.8. Gastric Ulcer Assessment; Ethanol Induction Model

All the aqueous and ethanol plant extract were evaluated for gastroprotective capability. The results showed that all the aqueous and ethanol plant extract were significantly ($P<0.05$) inhibited ulcer area against ethanol induction model in comparison to negative control group. Rats pretreated with 500 mg/kg of *C. xanthorrhiza* leaf ethanol extract CXLEE were protected stomach with 91.64 % while rats pretreated with *C. xanthorrhiza* leaf aqueous extract CXLAE were inhibited ulcer area with 74.00 %. Macroscobical examination of the gastric mucosa in a rat pre-treated with 5 mL/kg of 20 mg/kg OMP and 250 mg/kg and 500 mg/kg CXLEE showed moderate injuries in the gastric mucosa in comparison with CMC negative control group. It was also observed that histological examination of the stomach of rats pretreated with CMC suffered markedly extensive damage to the gastric mucosal layer with edema and leukocyte infiltration of the submucosal layer. Rats pre-treated with 5 ml/kg of 20 mg/kg omeprazole showed mild disruption to surface epithelium mucosa with mild edema and leukocyte infiltration of the submucosal layer. Meanwhile, rats pretreated with 500 mg/kg of CXLEE showed less destruction to the mucosal surface and mild edema and leukocyte infiltration in submucosal layer as shown in Fig. 5.

The p^H of gastric juice was recorded for all groups, the results showed that rats pretreated with negative control group (CMC and DW) have significantly ($P<0.05$) lower p^H (3.45 ± 0.13 and 3.60 ± 0.10 respectively) compared to other groups. While the p^H of gastric juice in the rats pretreated with positive control group OMP and all the plant extract in both aqueous extract (Fig. 4.3) and ethanolic extract were significantly ($P<0.05$) higher pH than negative control group. Rats pretreated with 20 mg/kg of OMP (6.84 ± 0.17) and 500 mg/kg of APLEE (7.18 ± 0.09) and PMLEE (7.22 ± 0.14) as in Table 8 showed elevation of p^H compared to other selected plants.

3.9. Comparative Studies

The antiulcer effect of curcuma xanthorhiza (roxb) was compared with traditional folk medicines used for the effectiveness against ulcer namely Maytenus robusta (Celastraceae), Pithecellobium Jiringa, Achryocline saturoides. The ethanol extract of each of the above plants were compared depending upon the data available under the headings shown in Table 8.

3.10. Medicinal review analysis

Table 9 established the antiulcer effect of curcuma xanthorhiza (roxb) was compared with traditional folk medicines used for the effectiveness against ulcer namely Maytenus robusta (Celastraceae), Pithecellobium Jiringa, Achryocline saturoides. The ethanol extract of each of the above plants were compared depending upon the data available under the following headings p^H, ulcer area, inhibiton %. Curcuma xanthorizha have resulted in the formation of high p^H i.e. 4.25 ±0.10* and 5.10±0.23* respectively at 250mg and 500 mg, indicating the inhibitory effect on gastric mucosa and movement of the p^H scale towards alkaline, indicating a better result when compared with Maytenus robusta which have less p^H i.e. 2.96±0.07* and 2.92±0.15* respectively at 250 mg and 500 mg. Also, while comparing the ulcer area inhibition % Curucuma xanthorhiza have proved to be more efficacious with percentage of 90.68 and 91.64 at 250mg and 500mg respectively, when compared with Prithecellobium Jiringa which have inhibition % of 72.17 and 80.55 at 250 mg and 500 mg respectively. Comparing similarly the data's of Achyrocline satureiodes which have an inhibition % of 58.8±11.5 and 86.2±12.2 at 250mg and 500 mg, which are largely at a low range when compared to that of Curucuma xanthorhiza.

3.11. Molecular docking analysis

On a global scale, molecular docking has been identified as a critical tool for drug design because it aims to explain several modules underlying protein-ligand interaction, which support the process by which proteins interact with small molecules (known as ligands) to form stable

Table 7
Biological activity and physicochemical parameters of CXZ.

Physicochemical Properties		Lipophilicity	
Form.	$C_{21}H_{20}O_6$	Log Po/w (iLOGP)	3.27
Mol. weight	368.38 g/mol	Log Po/w (XLOGP3)	3.20
Num. heavy atoms	27	Log Po/w (WLOGP)	3.15
Fract. Csp3	12	Log Po/w (MLOGP)	1.47
Num. rot. bonds	0.14	Log Po/w (SILICOS-IT)	4.04
Num. H-bond accpt.	8	Consensus Log Po/w	3.03
Num. H-bond donors	6	Log Po/w (iLOGP)	3.27
TPSA	93.06 Å^2	Class	Soluable
PK		**Medicinal Chemistry**	
GI abs.	High	PAINS	0 alert
BBB permeant	No	Brenk	2 alerts: beta_keto_anhydride, michael_acceptor_1
P-gp substrate	No	Lead like ness	No; 2 violations: MW>350, Rotors>7
CYP1A2 inhib.	No	Synthetic accessibility	2.97
CYP2C19 inhib.	No	**Water Solubility**	
CYP2C9 inhib.	Yes	Log_S_(ESOL)	-3.94
CYP2D6 inhib.	No	Solub.	4.22e-02 mg/ml; 1.15e-04 mol/l
CYP3A4 inhib.	Yes	Class	Soluble
Dr.likeness	Yes	Log_S_(Ali)	-4.83
Lipinski	No; 1 violation	Solub.	5.50e-03 mg/ml; 1.49e-05 mol/l
Ghose	Yes	Log_S_ (SILICOS-IT)	-4.45
Veber	No; 1 violation	Solub.	1.31e-02 mg/ml; 3.56e-05 mol/l
Egan	Yes		
Muegge	0.56		
Bio.av. Score	Yes		
Log Kp (skin permeation)	-6.28 cm/s		

Formula, Mol.weight: Molecular weight, Num: Number, Solub.: Solubility, Abs.: Absorption, Inhib.: Inhibitors, Bio.av.score: Bioavailability score, Dr.likeness: Druglikeness, PK: Pharmacokinetics, accpt: acceptor, rot.: rotatable, Fract.: Fraction.

complexes with biologically significant functions [45–50]. Contrarily, protein-ligand complexes are essential for a number of biological functions. In this case, the inhibition of the carbonic anhydrase enzyme is discussed, which is thought to be the main driver of the therapeutic benefits in evaluating ulcer illnesses. According to research by Chakravarty and colleagues [51], carbonic anhydrase interacted with three different sulfonamide drug structures to form complexes that were all bound in the enzyme's active site, but these complexes varied in the ways that their sulfamido groups interacted with the crucial zinc ion. As a result, the current research that led to the selection of this target receptor was made easier and further supported the existence of an active site in the enzyme. At the cellular level, the hydrogen bond plays a critical role in enhancing molecular interaction and compound structural integrity [52]. It also aids in compound solubility and gastrointestinal absorption into the body. Notably, as illustrated in Fig. 6, the active site loop of Lys213, Glu214, Lys149, and Ser217 was determined to be crucial for binding of the lead compound due to its substantial atomic displacements and intra-molecular hydrogen bonding as shown in Fig. 7. The orientation discrepancies of curcumin as well as variations in the inhibitory potencies of the compound was proposed to be caused by these interactions coupled with active site charge requirements. The native enzyme's Lys213, Glu214, Lys149, and Ser21767 active site residues, among others, were observed to form a hydrogen bond network with solvent molecules that was observed to be broken following binding to curcumin. In addition, Lys149 and Ser215 amino acid residues were seen in the interaction between the conventional drug (omeprazole) and the target receptor, which is determined to be comparable to that of curcumin and the target protein. These, however, imply that both amino acid residues are crucial for enhancing the lead compound's inhibitory potentials. However, it was determined that the omeprazole@1BZM interaction contained noteworthy pi-hydrogen bonds, pi sulphur, pi-alkyl, pi-pi T-shaped, and alkyl links. As both CXZ and omeprazole computed relatively identical binding affinities of -5.67 kcal/mol and -5.12 kcal/mol, respectively, this investigation relatively establish that curcumin could as well act as a proton pump inhibitor thus blocking precisely the carbonic anhydrase enzyme used in this investigation.

4. Conclusion

The spectroscopic and pharmaceutical investigations of the ligand were investigated theoretically and experimentally using DFT and the B3LYP/6-311++G(d,p) level of theory. Using NMR, FT-IR, and UV-Vis Spectroscopy studies, the plant extracts were extracted and characterized. Density functional theory (DFT) at the B3LYP/6-311++ G (d,p)

Table 8
p^H, ulcer area, inhibiton %.

		Maytenus robusta	*Curcuma xanthorhiza*	*Pithecellobium Jiringa*	*Achyrocline satureoides*
p^H	250mg	2.96 ± 0.07*	4.25 ± 0.10*	-	-
	500mg	2.92 ± 0.15*	5.10 ± 0.23*	-	-
Ulcer area (mm)2 (Mean ± S.E. M)	control	-			361.2 ± 51.3
	250mg	-	91.10 ± 9.29*	228.17 ± 1.51	25.9 ± 8.5
	500mg	-	81.70 ± 7.29*	156.33 ± 1.84	9.3 ± 8.3
Inhibition % (250mg)		-	90.68	72.17	58.8 ± 11.5
Inhibition % (500mg)		-	91.64	80.55	86.2 ± 12.2

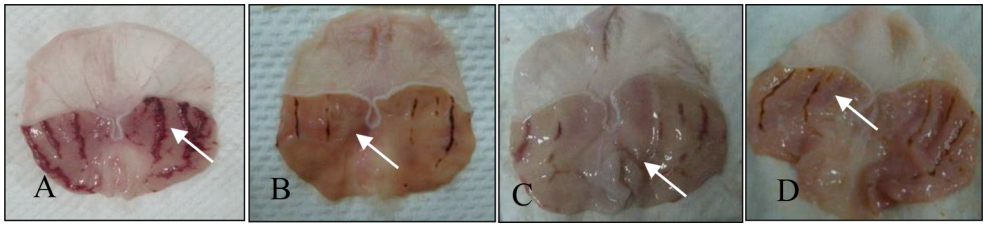

Fig. 5. Macroscopic observation of gastric wall in: (A) rats pre-treated with 5 mL/kg of CMC (negative control), (B) omeprazole (20 mg/kg) positive control group, (C) 5 mL/kg of 250 mg/kg CXLEE and (D) 500 mg/kg of CXLEE. Severe injuries were seen in the gastric mucosa in rats pre-treated with CMC. Injuries to the gastric mucosa were milder in rats pre-treated with omeprazole in comparison to the injuries seen in the CMC pre-treated rat. Moderate injuries are seen in the gastric mucosa (magnification: 1.8X). The white arrow indicates gastric lesion as shown in Fig. 6.

Table 9
Analysis of the medicinal review.

		Maytenus robusta	Curcuma xanthorhiza	Pithecellobium Jiringa	Achyrocline satureoides
p^H	250mg	2.96 ± 0.07*	4.25 ± 0.10*	-	-
	500mg	2.92 ± 0.15*	5.10 ± 0.23*	-	-
Ulcer area $(mm)^2$	control	-			361.2 ± 51.3
(Mean ± S.E.M)	250mg	-	91.10 ± 9.29*	228.17 ± 1.51	25.9 ± 8.5
	500mg	-	81.70 ± 7.29*	156.33 ± 1.84	9.3 ± 8.3
Inhibition % (250mg)		-	90.68	72.17	58.8 ± 11.5
Inhibition % (500mg)		-	91.64	80.55	86.2 ± 12.2

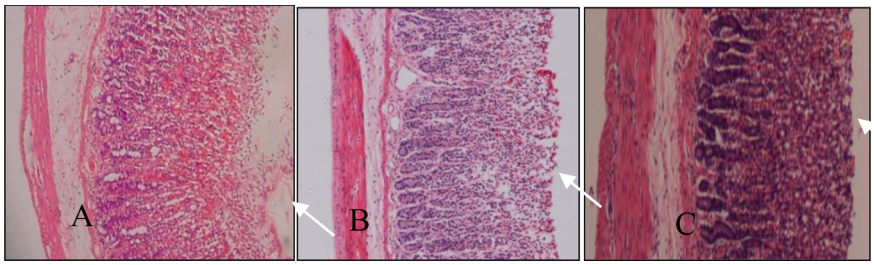

Fig. 6. Histological section of gastric mucosa in a rat pretreated with (A) 5 mL/kg of CMC (negative control), (B) 20 mg/kg of omeprazole and (C) 5 mL/kg of 500 mg/kg CXLEE (H&E stain 10x). Severe disruption at the epithelium and edema of the submucosal layer with leucocytes infiltration occurred (A). Mild disruption to the surface epithelium with mild edema and leucocytes infiltration of the submucosal layer (B) (H&E stain 10 x). White arrow represents surface epithelium and white arrow represents submucosal layer.

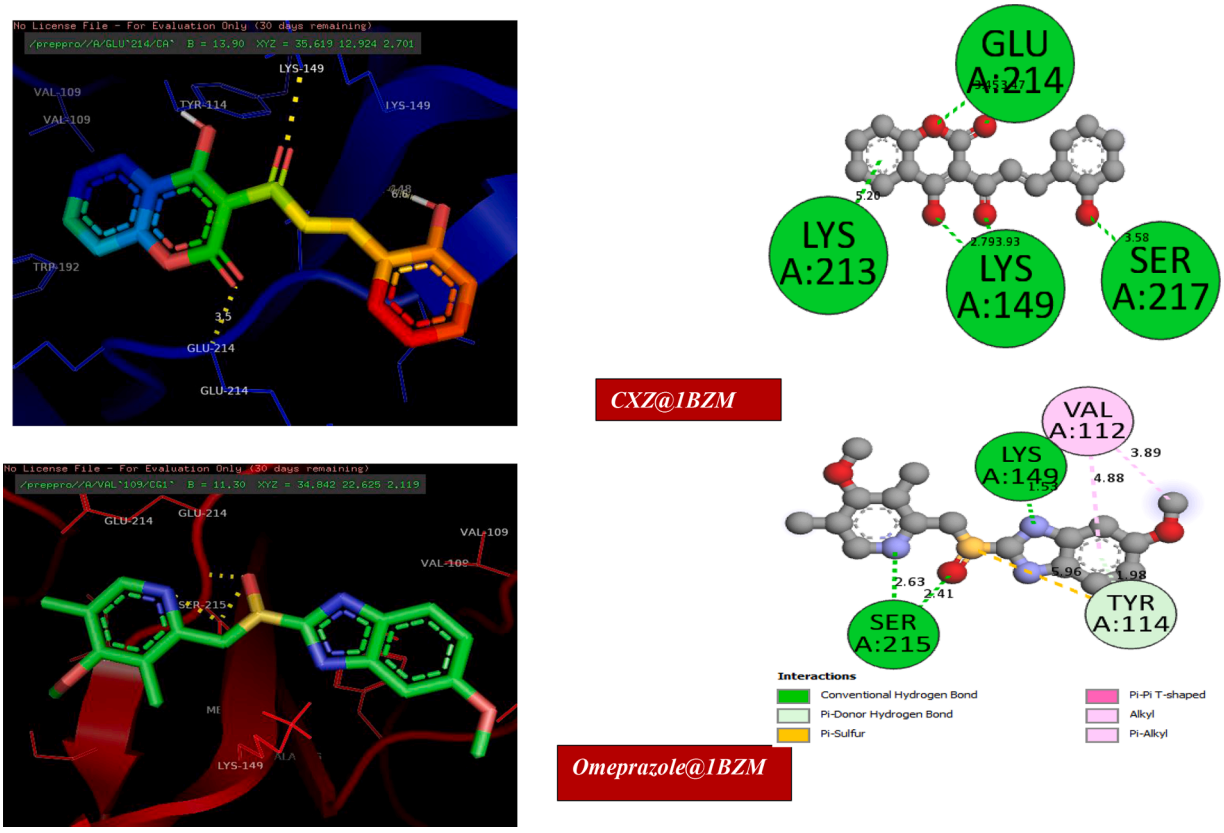

Fig. 7. 3D and 2D representation of CXZ and omeprazole docked with 1BZM.

level of theory was used to accomplish pre-geometry characterisation as well as theoretical analysis. To determine the molecular stability and chemical reactivity of the examined compounds, global descriptors at the same theoretical level were determined. Stabilization experiments were carried out to adequately assess the stability of the complex, and the results revealed that the charge delocalization from the sigma (σ) to anti-sigma (σ)*) molecular orbital was primarily responsible for the molecular stability of the investigated moleculeAccording to the estimated UV-Vis spectroscopy analysis, all absorption occurred in the visible region (400–700 nm), which is consistent with the experimentally found maximum. These findings imply that the compound under investigation may be attributed to the aromatic, amino benzoate anion, monohydrate, and oxalate moiety, respectively. According to the FMO investigations, the molecule under investigation computed a very significant energy gap of 3.437 eV, which when compared to other literature suggests that this compound has enough biological capabilities. From the natural bond analysis, it can be seen that the examined compound had the highest donor to acceptor interaction from (donor) σC20 -

C21 → σ*C28 - H30 (acceptor), σC18 - C20 → σ*C26 - C28, σC20 - H35→ *σC26 - C28 which is found to have the highest stabilization energy of 594.04 Kcal/mol. Significantly, the improved molecular structure and electronic structural analysis supported the molecular electrostatic potential (MEP) finding that the charge transfer actually occurred within the moleculeThe lead compound is evaluated as an effective phyto-compound with a better efficacy against the pharmaceutical targets based on all reports from the HOMO-LUMO, chemical reactivity, charge distribution (mulliken population analysis and MESP plots), and docking studies. As result from the topology and admet properties explicates that CXZ molecule exhibited good ADMET properties and therefore suggests its suitability as potential plant based drug.

Funding

This research was not funded by any Governmental or Non-governmental agency.

CRediT authorship contribution statement

Suhailah Wasman Qader: Project conceptualization, design, and supervision. **A. Suvitha, Mehmet Ozdemir** and **Anu Sai Ram NSA:** Writing, results extraction, analysis, and manuscript first draft. **Innocent Benjamin:** supervision, Manuscript revision, review, and proof-reading, Writing, editing, and analysis. **Martilda U. Akem, Eze Frank Ahuekwe and Emereze C. Eluwa:** Writing, editing, and analysis.

Declaration of Competing Interest

All authors declare zero financial or inter-personal conflict of interest that could have influenced the research work or results reported in this research paper.

Data availability

Data will be made available on request.

Supplementary materials

Supplementary material associated with this article can be found, in the online version, at doi:10.1016/j.chphi.2022.100130.

References

[1] A.M. Sontsa-Donhoung, M. Bahdjolbe, D. Nwaga, Selecting Endophytes for Rhizome Production, Curcumin Content, Biocontrol Potential, and Antioxidant Activities of Turmeric (Curcuma longa), Biomed Res. Int. 2022 (2022).
[2] B. Jyotirmayee, G. Mahalik, A review on selected pharmacological activities of Curcuma longa L, Int. J. Food Prop. 25 (1) (2022) 1377–1398.
[3] Klau, M. E., Rohaeti, E., Rafi, M., Artika, I. M., Ambarsari, L., & Nurcholis, W. (2022). Metabolite Profiling of Curcuma zanthorrhiza Varieties Grown in Different Regions Using UHPLC-Q-Orbitrap-HRMS and Chemometrics Analysis.
[4] S. Fuloria, J. Mehta, A. Chandel, M. Sekar, N.N.I.M. Rani, M.Y. Begum, N. K. Fuloria, A comprehensive review on the therapeutic potential of Curcuma longa Linn. in relation to its major active constituent curcumin, Front. pharmacol. 13 (2022).
[5] M.F.R. Syaban, R.F. Muhammad, B. Adnani, G.F.A. Putra, N.E. Erwan, S. D. Arviana, D.B. Kurniawan, Molecular Docking Studies of Interaction Curcumin against Beta-secretase 1, Amyloid A4 Protein, Gamma-secretase and Glycogen Synthase Kinase-3β as Target Therapy for Alzheimer Disease, Res. J. Pharm. Technol. 15 (7) (2022) 3069–3074.
[6] S.S. Panda, Q.L. Tran, P. Rajpurohit, G.G. Pillai, S.J. Thomas, A.E. Bridges, …, B. L. Lokeshwar, Design, Synthesis, and Molecular Docking Studies of Curcumin Hybrid Conjugates as Potential Therapeutics for Breast Cancer, Pharmaceuticals 15 (4) (2022) 451.
[7] M. Ahmed, M.A. Qadir, A. Hameed, M.N. Arshad, A.M. Asiri, M. Muddassar, Sulfonamides containing curcumin scaffold: Synthesis, characterization, carbonic anhydrase inhibition and molecular docking studies, Bioorganic chemistry 76 (2018) 218–227.
[8] V. Furlan, J. Konc, U. Bren, Inverse molecular docking as a novel approach to study anticarcinogenic and anti-neuroinflammatory effects of curcumin, Molecules 23 (12) (2018) 3351.
[9] M. Kumar, K.K. Sodhi, D.K. Singh, Addressing the potential role of curcumin in the prevention of COVID-19 by targeting the Nsp9 replicase protein through molecular docking, Archives of microbiology 203 (4) (2021) 1691–1696.
[10] H. Hussain, S. Ahmad, S.W.A. Shah, M. Ghias, A. Ullah, S.U. Rahman, …, S. Alghamdi, Neuroprotective Potential of Synthetic Mono-Carbonyl Curcumin Analogs Assessed by Molecular Docking Studies, Molecules 26 (23) (2021) 7168.
[11] W. Cao, X. Chen, Y. Chin, J. Zheng, P.E. Lim, C. Xue, Q. Tang, Identification of curcumin as a potential α-glucosidase and dipeptidyl-peptidase 4 inhibitor: Molecular docking study, in vitro and in vivo biological evaluation, J. Food Biochem. 46 (3) (2022) e13686.
[12] M. Govindammal, M. Prasath, S. Kamaraj, S. Muthu, M. Selvapandiyan, Exploring the molecular structure, vibrational spectroscopic, quantum chemical calculation and molecular docking studies of curcumin: A potential PI3K/AKT uptake inhibitor, Heliyon 7 (4) (2021) e06646.
[13] R. Suravajhala, A. Parashar, G. Choudhir, A. Kumar, B. Malik, V.A. Nagaraj, P. B. Kishor, Molecular docking and dynamics studies of curcumin with COVID-19 proteins, Netw. Model. Anal. Health Inform. Bioinform. 10 (1) (2021) 1–10.
[14] A. Dwivedi, A. Kumari, M. Aarthy, S.K. Singh, M. Ojha, S. Jha, N.S. Jha, Spectroscopic and molecular docking studies for the binding and interaction aspects of curcumin-cysteine conjugate and rosmarinic acid with human telomeric G-quadruplex DNA, Netw. Model. Anal. Health Inform. Bioinform. 182 (2021) 1463–1472.
[15] R. Debroy, S. Ramaiah, MurC ligase of multi-drug resistant Salmonella Typhi can be inhibited by novel Curcumin derivative: Evidence from Molecular Docking and Dynamics Simulations, Int. J. Biochem. Cell Biol. (2022), 106279.
[16] G. Moreno-Q, A. Herrera-R, A.F. Yepes, T.W. Naranjo, W. Cardona-G, Proapoptotic Effect and Molecular Docking Analysis of Curcumin–Resveratrol Hybrids in Colorectal Cancer Chemoprevention, Molecules 27 (11) (2022) 3486.
[17] N.M. O'boyle, A.L. Tenderholt, K.M. Langner, Cclib: a library for package-independent computational chemistry algorithms, J. Comput. Chem. 29 (5) (2008) 839–845.
[18] Gaussian09, R. A. (2009). 1, mj frisch, gw trucks, hb schlegel, ge scuseria, ma robb, jr cheeseman, g. Scalmani, v. Barone, b. Mennucci, ga petersson et al., gaussian. *Inc., Wallingford CT, 121*, 150-166.
[19] R. Dennington., T.A. Keith., & J. M. Millam., GaussView 6.0. 16. *Semichem Inc.: Shawnee Mission, KS, USA*. HyperChem, T. (2001). HyperChem 8.07, HyperChem Professional Program. *Gainesville, Hypercube*. (2016).
[20] Z. Parsaee, K. Mohammadi, Synthesis, characterization, nano-sized binuclear nickel complexes, DFT calculations and antibacterial evaluation of new macrocyclic Schiff base compounds, J. Mol. Struct. 1137 (2017) 512–523.
[21] O.A. El-Gammal, T.H. Rakha, H.M. Metwally, G.M. Abu El-Reash, Synthesis, characterization, DFT and biological studies of isatinpicolinohydrazone and its Zn (II), Cd(II) and Hg(II) complexes, Spectrochim. Acta A Mol. Biomol. Spectrosc. 127 (2014) (2014) 144–156.
[22] R.P. Dubey, U.H. Patel, S.B. Pandya, K.P. Chaudhary, B.N. Socha, Cadmium complex of sulfathiazole dihydrate with secondary ligand pyridine: structure, DFT studies, Hirshfeld surface analysis and antimicrobial activity, Indian J. Phys. (2019), https://doi.org/10.1007/s12648-019-01680-8.
[23] B.F. Rizwana, J.C. Prasana, C.S. Abraham, S. Muthu, Spectroscopic investigation, hirshfeld surface analysis and molecular docking studies on anti-viral drug entecavir, J. Mol. Struct. 1164 (2018) 447–458.
[24] J. Ebrahimi, M. Ghorbanzadeh Ahangari, M. Jahanshahi, Computational studies at the density functional theory (DFT) level about the surface functionalization of hexagonal monolayers by chitosan monomer, Appl. Surf. Sci. 440 (2018) 778–789.
[25] Y. Cao, A. Khan, H. Balakheyli, A.N.K. Lup, M.R. Taghartapeh, H. Mirzaei, S. R. Khandoozi, A. Soltani, M. Aghaei, F. Heidari, S.M. Sarkar, A.B. Albadarin, Penicillamine functionalized B12N12 and B12CaN12 nanocages act as potential inhibitors of proinflammatory cytokines: A combined DFT analysis, ADMET and molecular docking study, Arab. J. Chem. 14 (2021), 103200.
[26] Mahmood, A. Albo Hay Allah, Asim A. Balakit, Hamida Idan Salman, Ali Ahmed Abdulridha, and Yusuf Sert,". *New Heterocyclic Compound as Carbon Steel Corrosion Inhibitor in*, 1, 1-23.
[27] N. Dege, H. Gökce, O.E. Doğan, G. Alpaslan, T. Ağar, S. Muthu, Y. Sert, Quantum computational, spectroscopic investigations on N-(2-((2-chloro-4, 5-dicyano-phenyl) amino) ethyl)-4-methylbenzenesulfonamide by DFT/TD-DFT with different solvents, molecular docking and drug-likeness researches, Colloids Surf. A: Physicochem. Eng. Asp. 638 (2022), 128311.
[28] M. Gümüş, Ş.N. Babacan, Y. Demir, Y. Sert, İ. Koca, İ. Gülçin, Discovery of sulfadrug–pyrrole conjugates as carbonic anhydrase and acetylcholinesterase inhibitors, Archiv. Der. Pharmazie 355 (1) (2022), 2100242.
[29] I. Mahmudov, Y. Demir, Y. Sert, Y. Abdullayev, A. Sujayev, S.H. Alwasel, I. Gulcin, Synthesis and inhibition profiles of N-benzyl-and N-allyl aniline derivatives against carbonic anhydrase and acetylcholinesterase–A molecular docking study, Arab. J. Chem. 15 (3) (2022), 103645.
[30] E.A. Eno, H. Louis, P. Ekoja, I. Benjamin, S.A. Adalikwu, M.M. Orosun, E. C. Agwamba, Experimental and computational modeling of the biological activity of benzaldehyde sulphur trioxide as a potential drug for the treatment of Alzheimer disease, J. Indian Chem. Soc. 99 (7) (2022), 100532.
[31] B.K. Das, P.V. Pushyaraga, D. Chakraborty, Computational insights into factor affecting the potency of diaryl sulfone analogs as Escherichia coli dihydropteroate synthase inhibitors, Comput. Biol. Chem. 78 (2019) 37–52.
[32] I. Benjamin, A.D. Udoikono, H. Louis, E.C. Agwamba, T.O. Unimuke, A.E. Owen, A. S. Adeyinka, Antimalarial potential of naphthalene-sulfonic acid derivatives:

Molecular electronic properties, vibrational assignments, and in-silico molecular docking studies, J. Mol. Struct. (2022), 133298.
[33] E.A. Eno, J.I. Mbonu, H. Louis, F.S. Patrick-Inezi, T.E. Gber, T.O. Unimuke, O. E. Offiong, Antimicrobial activities of 1-phenyl-3-methyl-4-trichloroacetyl-pyrazolone: Experimental, DFT studies, and molecular docking investigation, J. Indian Chem. Soc. 99 (7) (2022), 100524.
[34] E.C. Agwamba, I. Benjamin, H. Louis, A.D. Udoikono, A.T. Igbalagh, T. C. Egemonye, A.S. Adeyinka, Antitubercolusic Potential of Amino-(formylphenyl) Diazenyl-Hydroxyl and Nitro-Substituted Naphthalene-Sulfonic Acid Derivatives: Experimental and Theoretical Investigations, Chemistry Africa (2022) 1–17.
[35] E.C. Agwamba, A.D. Udoikono, H. Louis, E.U. Udoh, I. Benjamin, A.T. Igbalagh, U. B. Ushaka, Synthesis, characterization, DFT studies, and molecular modeling of azo dye derivatives as potential candidate for trypanosomiasis treatment, Chem. Phys. Impact (2022), 100076.
[36] H.O. Edet, H. Louis, I. Benjamin, M. Gideon, T.O. Unimuke, S.A. Adalikwu, A. S Adeyinka, Hydrogen storage capacity of C12X12 (X= N, P, and Si), Chem. Phys. Impact (2022), 100107.
[37] E.C. Agwamba, H. Louis, I. Benjamin, C.G. Apebende, T.O. Unimuke, H.O. Edet, …, A.S. Adeyinka, (E)-2-((3-Nitrophenyl) Diazenyl)-3-Oxo-3-Phenylpropanal: Experimental, DFT Studies, and Molecular Docking Investigations, Chemistry Africa (2022) 1–17.
[38] H. Louis, D.E. Charlie, I.O. Amodu, I. Benjamin, T.E. Gber, E.C. Agwamba, A. S. Adeyinka, Probing the Reactions of Thiourea (CH4N2S) with Metals (X= Au, Hf, Hg, Ir, Os, W, Pt, and Re) Anchored on Fullerene Surfaces (C59X), ACS Omega (2022).
[39] T.E. Gber, H. Louis, A.E. Owen, B.E. Etinwa, I. Benjamin, F.C. Asogwa, …, E.A. Eno, Heteroatoms (Si, B, N, and P) doped 2D monolayer MoS 2 for NH 3 gas detection, RSC Advances 12 (40) (2022) 25992–26010.
[40] F.C. Asogwa, E.C. Agwamba, H. Louis, M.C. Muozie, I. Benjamin, T.E. Gber, A. I. Ikeuba, Structural benchmarking, density functional theory simulation, spectroscopic investigation and molecular docking of N-(1H-pyrrol-2-yl) methylene)-4-methylaniline as castration-resistant prostate cancer chemotherapeutic agent, Chem. Phys. Impact 5 (2022), 100091.
[41] E.C. Agwamba, A.D. Udoikono, H. Louis, E.U. Udoh, I. Benjamin, A.T. Igbalagh, …, U.B. Ushaka, Synthesis, characterization, DFT studies, and molecular modeling of azo dye derivatives as potential candidate for trypanosomiasis treatment, Chemical Physics Impact (2022), 100077.
[42] B.E. Inah, L. Hitler, B. Innocent, T. Unimuke, A.S. Adeyinka, Computational study on the interactions of functionalized C24NC (NC= C,-OH,-NH2,–COOH, and B) with chloroethylphenylbutanoic acid, Can. J. Chem. (2022).
[43] J.G. Hill, A.C. Legon, Radial Potential Energy Functions of Linear Halogen-Bonded Complexes YX··· ClF (YX= FB, OC, SC, N2) and the Effects of Substituting X by Second-Row Analogues: Mulliken Inner and Outer Complexes, J. Phys. Chem. A 126 (16) (2022) 2511–2521.
[44] G. Golding Sheeba, D. Usha, M. Amalanathan, M. Sony Michael Mary, H. MarshanRobert, Molecular structure, vibrational spectroscopic, frontier molecular orbital and natural bond orbital analysis of anti-cancer drug 6-chloro-3-pyridine carbonitrile, Spectrosc. Lett. 54 (6) (2021) 419–436.
[45] M. Fizer, O. Fizer, Theoretical study on charge distribution in cetylpyridinium cationic surfactant, J. Mol. Model. 27 (7) (2021) 1–11.
[46] M.A.A. Tayeb, N. Tchouar, F.A. Miannay, A. Idrissi, Effect of the mixture composition of C4mimBF4/acetonitrile on the charge transfer in Coumarin 153: DFT and TD-DFT analysis, J. Mol. Liq. 339 (2021), 116830.
[47] M.A.M. El-Mansy, A. Suvitha, B. Narayana, Exploring crystal, electronic, optical and NLO properties of ethyl 4-(3, 4-dimethoxy phenyl)-6-methyl-2-thioxo-1, 2, 3, 4-tetrahydro pyrimidine-5-carboxylate (MTTHPC), Opt. Quantum Electron 53 (8) (2021) 1–16.
[48] M.D. Mohammadi, H.Y. Abdullah, A. Suvitha, The adsorption of 1-chloro-1, 2, 2, 2-tetrafluoroethane onto the pristine, Al-, and Ga-doped boron nitride nanosheet, Iran J. Sci. Technol. Trans. A Sci. 45 (4) (2021) 1287–1300.
[49] D.E. Pires, T.L. Blundell, D.B. Ascher, pkCSM: predicting small-molecule pharmacokinetic and toxicity properties using graph-based signatures, J. Med. Chem. 58 (9) (2015) 4066–4072.
[50] A. Daina, O. Michielin, V. Zoete, SwissADME: a free web tool to evaluate pharmacokinetics, drug-likeness and medicinal chemistry friendliness of small molecules, Scientific reports 7 (1) (2017) 1–13.
[51] S. Chakravarty, K.K. Kannan, Drug-protein interactions: refined structures of three sulfonamide drug complexes of human carbonic anhydrase I enzyme, J. Mol. Biol. 243 (2) (1994) 298–309.
[52] P.P. Venugopal, B.K. Das, E. Soorya, D. Chakraborty, Effect of hydrophobic and hydrogen bonding interactions on the potency of ß-alanine analogs of G-protein coupled glucagon receptor inhibitors, Proteins: Struct. Funct. Genet. 88 (2) (2020) 327–344.